Article ID: 1000-324X(2015)11-1223-05 **DOI:** 10.15541/jim20150251

$LaFe_{1-x}Mg_xO_3$ Ultrafine Powders Synthesized by Solution Combustion and Its Photocatalytic Performances

LI Jia-Ke, LIU Xin, HUANG LI-Qun, WANG Yan-Xiang

(School of Materials Science and Engineering, Jingdezhen Ceramic Institute, Jingdezhen 333403, China)

Abstract: Mg^{2+} doped $LaFeO_3$ ultrafine powders were synthesized by solution combustion method. Effects of Mg^{2+} doping content on phase composition, microstructure and photocatalytic performances of the synthesized powders were investigated by XRD, SEM, BET, and UV-Vis. The results show that Mg^{2+} substitutes for Fe^{3+} to form $LaFe_{1-x}Mg_xO_3$ ($0 \leqslant x \leqslant 0.2$) limited solid solution. When Mg^{2+} doping content is 0.1, $LaFe_{0.9}Mg_{0.1}O_3$ powder has a maximum specific surface area (43.46 m^2/g) and smaller particle size (100 nm and 150 nm in diameter and length direction, respectively). It has the best photocatalytic ability with photodegradation efficiency of 75.2% to methyl orange (10 mg/L) under high-pressure mercury lamp irradiation for 180 min. It increases 26.5% than that of the pure $LaFeO_3$ under the same experimental conditions, and the reaction may be described as the pseudo first order kinetics equation.

Key words: $LaFeO_3$; Mg^{2+} doping; solution combustion; photocatalytic performances

Rare-earth perovskite-type oxides have attracted wide attention of domestic and overseas scholars because they own unique properties, such as photocatalytic[1], piezoelectric[2-3] and optical[4], so they may be applied in the field of sewage treatment[1], sensors[5] and electrode materials[6-7], *etc*. Among many rare-earth perovskite-type oxides, due to $LaFeO_3$ has special optical, electromagnetic and catalytic properties, so it plays an important role in many respects.

$LaFeO_3$ as photocatalyst has been reported as the candidate for the degradation of pollutants and hydrogen generation. Hu, *et al*[8]synthesized $LaFeO_3$ powder by glucose Sol-Gel method and investigated its photocatalytic ability to p-chlorophenol degradation, and photocatalytic efficiency reaches 49.0% under visible light irradiation for 300 min. Moreover, Parida, *et al*[9] synthesized nanocrystalline $LaFeO_3$ for water decomposition by Sol-Gel auto-combustion method. The result showed that the highest amount of H_2 and O_2 evolved in 180 min over the $LaFeO_3$ activated at 500℃ was recorded to 1290 μmol and 640 μmol, respectively.

At present, there are many kinds of methods for preparation of ultrafine powder, such as Sol-Gel[10-11], coprecipitation[12], hydrothermal[13] and combustion method[14], *etc*. Among the above preparation technologies, solution combustion method is a new method for synthesis of ultrafine powder. It has many advantages, such as low synthesized temperature, simple process conditions, easy-control preparation process, short reaction time, and the synthesized powder with small and uniform particle size[15-16]. In order to improve photocatalytic efficiency of semiconductor materials in the UV-Vis region, various methods have been employed, such as metal and/or non-metal ion doping[1], noble metal deposition and semiconductor coupling[17], *etc*. Li, *et al*[1] synthesized Ca-doped $LaFeO_3$ powder by a reverse microemulsion method, and the results showed that partial substitution of La^{3+} with Ca^{2+} could decrease the crystalline size, so photocatalytic activity is increased.

In this study, Mg^{2+} doped $LaFeO_3$ ultrafine powers were synthesized by solution combustion method. By Mg^{2+} doped in $LaFeO_3$, it may refine grain and increase specific surface area of the synthesized powders. Moreover, oxygen vacancies were formed due to Mg^{2+} instead of Fe^{3+}, so promote separation of photoelectrons and holes. Effects of Mg^{2+} doping content on phase composition, microstructure and photocatalytic performances of $LaFe_{1-x}Mg_xO_3$ ($0 \leqslant x \leqslant 0.2$) were investigated by means of BET, XRD, SEM and UV-Vis, and preparation parameters were optimized.

1 Experimental

1.1 Preparation of $LaFe_{1-x}Mg_xO_3$

$La(NO_3)_3 \cdot 6H_2O$, $Fe(NO_3)_3 \cdot 9H_2O$, $Mg(NO_3)_2 \cdot 6H_2O$ and

Received date: 2015-05-27; **Modified date:** 2015-07-09; **Published online:** 2015-09-10
Foundation item: International Science & Technology Cooperation Project of China (2013DFA51000); National Natural Science Foundation of China (51462015)
Biography: LI Jia-Ke(1973-), male, PhD, associate professor. E-mail: jiakeli.jci@163.com

sucrose ($C_{12}H_{22}O_{11}$) are of analytical grade, and are used without further purification. According to the principle of the propellant chemistry[15-16], assuming that CO_2, H_2O and N_2 are the only gaseous products, combustion reaction can be represented by Eq. (1). Various raw materials were weighed according to stoichiometric ratio (see Eq. (1)) and dissolved in deionized water. In precursor solution, La^{3+} concentration is 0.3 mol/L, and Fe^{3+} and Mg^{2+} concentration were determined by Eq. (1). A certain volume of precursor solution was taken to a refractory crucible and then placed in a furnace at 500℃. Subsequently, combustion reaction occurred, and the powders were obtained after the completion of combustion reaction. Finally, the powders were heat-treated at 900℃ for 60 min.

$$\begin{aligned}&\mathrm{La(NO_3)_3}+(1-x)\mathrm{Fe(NO_3)_3}+x\mathrm{Mg(NO_3)_2}+\\&\frac{5-x}{8}\mathrm{C_{12}H_{22}O_{11}}+\frac{3x}{2}\mathrm{O_2}\xrightarrow{\text{Igniting}}\\&\mathrm{LaFe_{1-x}Mg_xO_3}+\frac{15}{2}\mathrm{CO_2}+\frac{55-11x}{8}\mathrm{H_2O}+\frac{6-x}{2}\mathrm{N_2}\end{aligned}\quad(1)$$

1.2 Characterization

Phase compositions of the synthesized powders were analyzed on a D8 Advance X diffractometer with Cu Kα radiation (λ = 0.15406 nm), and the step size was 0.03 °/s. Specific surface area of the synthesized powders was studied by BET (Brunauer- Emmett-Teller) method with an ASAP-2020 automatic physical and chemical adsorption analyzer. A field emission SEM (JSM-6700F) was used to investigate microstructures of the synthesized powders.

Photodegradation experiments were performed in the self-made device. Methyl orange solution (concentration 10 mg/L) was used as simulates degradable substance. Light source was high-pressure mercury lamp (125 W, main wavelength 365 nm), and the distance from the surface of solution to the light was about 10 cm. The synthesized powders (0.1 g) was poured into 100 mL methyl orange solution and placed to the reactor, stirred in darkroom for 30 min in order to reach its adsorption and desorption equilibrium, then turned on the mercury lamp. After that, a small amount of this solution was taken for degradation analysis for each 30 min and separated using centrifuge. Absorbance of the solution was measured using spectrophotometer (detection wavelength 464 nm). The concentration of methyl orange was calculated by absorbance, and degradation efficiency was obtained by following formula (Eq. (2)):

$$A=\frac{C_0-C}{C_0}\times 100\% \quad (2)$$

A — Degradation efficiency of methyl orange

C_0 — Initial concentration of methyl orange

C— Concentration of methyl orange after degradation

2 Results and discussion

2.1 Phase evolution

Figure 1 shows XRD patterns of the synthesized powders with different Mg^{2+} doping contents. It can be seen from Fig. 1 that all patterns show $LaFeO_3$ characteristic diffraction peaks (JCPDS 37-1493). These indicate that $LaFeO_3$ have been synthesized with perovskite structure. Moreover, magnesium compounds do not appear in the XRD patterns. This indicates that Mg^{2+} enters the lattice position of $LaFeO_3$ and forms solid solution of $LaFe_{1-x}Mg_xO_3$. This is because Mg^{2+} radius (r=0.072 nm) is close to Fe^{3+} radius (r=0.064 nm), Mg^{2+} may replace the position of Fe^{3+} in $LaFeO_3$. Moreover, due to the valence of Mg^{2+} and Fe^{3+} is different, $LaFe_{1-x}Mg_xO_3$ is a kind of limited solid solution[17].

It also can be seen from Fig. 1 that the intensity of the diffraction peaks are weakened and the half peaks width widened with the increase of Mg^{2+} doping content. This is due to crystal lattice of $LaFeO_3$ occurs distortion with Mg^{2+} doping, the degree of crystallization of the synthesized powders is decreased.

2.2 Microstructure analysis and specific surface area

SEM images of the synthesized powders with Mg^{2+} different doping contents are shown in Fig. 2. It can be seen from Fig. 2 that the powders show short rod-like and average particle size becomes smaller both in the length and the diameter direction with the increase of Mg^{2+} doping content in $LaFeO_3$. The pure $LaFeO_3$, average particle size is 150 nm and 200 nm in the diameter and length direction (Fig. 2(a)), respectively. When Mg^{2+} doping content is 0.1 (x=0.1), average particle size of $LaFe_{0.9}Mg_{0.1}O_3$ is reduced to 100 nm and 150 nm in the diameter and length direction (Fig. 2(c)), respectively. When Mg^{2+} doping content is 0.2, average particle size of $LaFe_{0.8}Mg_{0.2}O_3$ is reduced to 80 nm and 120 nm in the diameter and length direction (Fig. 2(d)),

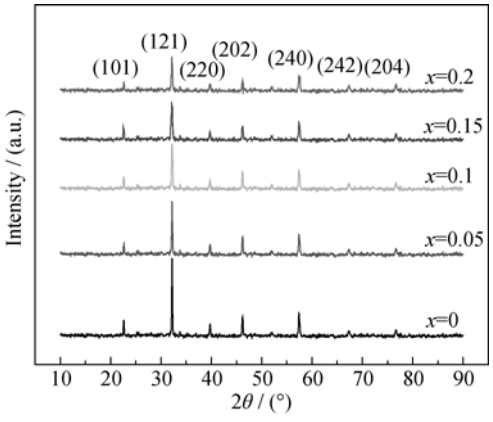

Fig. 1 XRD patterns of the synthesized powders with different Mg^{2+} doping contents

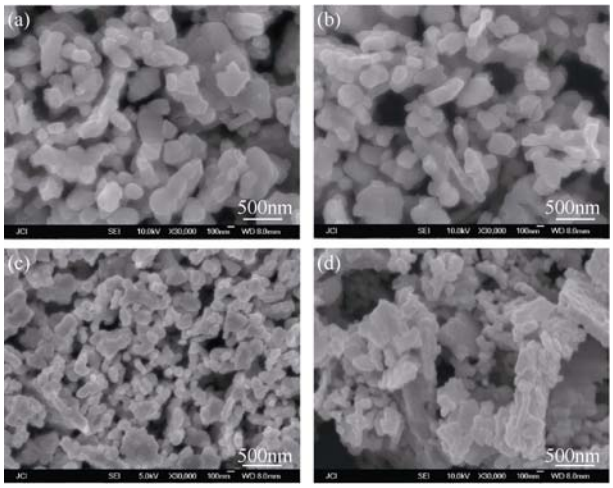

Fig. 2　SEM images of $LaFe_{1-x}Mg_xO_3$ powders
(a) x=0; (b) x=0.05; (c) x=0.1; (d) x=0.2

respectively. In addition, it can also be seen from Fig. 2, particle agglomeration of the synthesized powders is greatly intensified with the increase of Mg^{2+} doping content from 0.1 to 0.2. Due to Mg^{2+} as a kind of impurity added to $LaFeO_3$, it may inhibit the crystal growth of $LaFeO_3$, so particle size decreases with the increase of Mg^{2+} doping content. Moreover, the synthesized powders with smaller particle size cause agglomeration easily during the heat-treatment.

Table 1 shows specific surface area of the synthesized powders with Mg^{2+} doping different content. It can be seen from Table 1 that specific surface area of the powders gradually increases with the increase of Mg^{2+} doping content. When Mg^{2+} doping content is 0.1, specific surface area of the powders reaches maximum value of 43.46 m^2/g, which is two times more than that of $LaFeO_3$. With the further increase of doping content from 0.1 to 0.2, specific surface area of the powders decreases. When Mg^{2+} doping content is 0.2, specific surface area of the powders only is 28.82 m^2/g. With the increase of doping content, it causes the decrease of average particle size of the powders; at the same time, it also intensifies the particle agglomeration of the powders during the heat-treatment (see Fig. 2). Therefore, a suitable doping content is very important to refine grain and increase specific surface area of the powers. The above analyses results for the synthesized powders about their microstructure, specific surface area and XRD are consistent.

Table 1　Specific surface area of the synthesized powders with Mg^{2+} different doping content

Mg^{2+} doping content, x	Specific surface area/($m^2 \cdot g^{-1}$)
x=0	20.63
x=0.05	24.52
x=0.1	43.46
x=0.15	33.57
x=0.2	28.82

2.3　Photocatalytic performances

Figure 3 shows photocatalytic performances of the synthesized powders with Mg^{2+} different doping content. It can be seen from Fig. 3, for all the synthesized powders as photocatalyst, degradation efficiency of methyl orange gradually increases with the increase of illumination time. These indicate that the synthesized powders own photocatalytic ability. Moreover, it can also be seen from Fig. 3, the powders with Mg^{2+} different doping content, photocatalytic ability is very different. With the increase of Mg^{2+} doping content in $LaFeO_3$, photocatalytic ability of the synthesized powders first increases and then decreases, and Mg^{2+} doping content is 0.1, the synthesized powder ($LaFe_{0.9}Mg_{0.1}O_3$) owns the best photocatalytic ability. When illumination time is 180 min, degradation efficiency of methyl orange arrives at a maximum value of 75.2%, and it is increased 54.4% than that of $LaFeO_3$.

The above experimental results can be explained as follows. Due to Mg^{2+} doped in $LaFeO_3$, it may refine grain, and increases specific surface area of the synthesized powders, so that adsorption capacity of the powders to methyl orange is increased. At the same time, smaller crystal size also intensifies agglomeration of the powders during heat treatment (see Fig. 2), so a suitable doping content is very important to increase specific surface area of the powers. Moreover, due to chemical valence between Mg^{2+} and Fe^{3+} is different, this causes oxygen vacancies ($V_o^{\cdot\cdot}$) in $LaFe_{1-x}Mg_xO_3$ (see Eq. 3)[17], and they may capture photoelectrons and promote separation of photoelectrons and holes. Therefore, photocatalytic ability of the powders is increased. However, when doping content is too high, the dopant may act as an electron-hole recombination center and decrease photocatalytic activity[18].

$$2MgO \xrightarrow{LaFeO_3} 2Mg'_{Fe} + V_o^{\cdot\cdot} + 2O_o \qquad (3)$$

Li, *et al*[19] synthesized $LaCoO_3$ ultrafine particle by template method, and photocatalytic test result shows

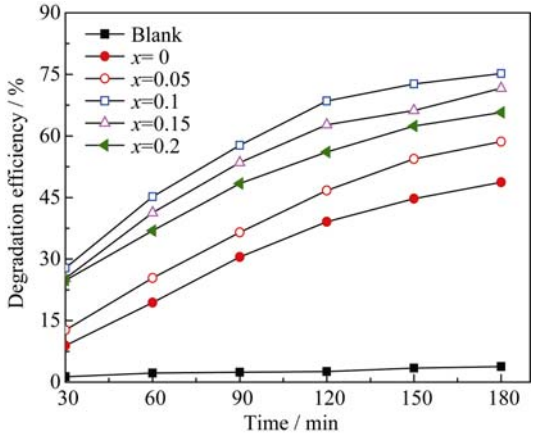

Fig. 3　Photocatalytic performance of the synthesized powders with different Mg^{2+} doping contents

that photodegradation efficiency of methyl orange (10 mg/L) is less than 10% under UV lamp irradiation for 180 min. By comparing the results of two experiments, the as-synthesized $LaFeO_3$ or Mg^{2+} doped $LaFeO_3$ has higher photocatalytic ability. It attributes to high specific surface area and oxygen vacancies ($V_o^{\cdot\cdot}$) of Mg^{2+} doped $LaFeO_3$.

In order to study on photocatalytic reactive kinetics of the synthesized powders to methyl orange, some data processed are shown in Fig. 4. It can be seen from Fig. 4 that there is a good linear relationship between $\ln(C_0/C_t)$ and time (t) , and correlation coefficient R^2 is nearly equal to 1 (see Table 2). These indicate that photocatalytic reaction accords with the pseudo first order kinetics equation.

Moreover, according to Langmuir-Hinshelwood (L-H) kinetic model theory[20], photocatalytic kinetic reaction and rate constant can be obtained from Fig. 4, and they are shown in Table 2. The synthesized powders with Mg^{2+} different doping content have different reactive rate constants (k) to degrade methyl orange. $LaFe_{0.9}Mg_{0.1}O_3$ (x=0.1) owns the highest k value, so it has the best photocatalytic ability to methyl orange; $LaFeO_3$ owns the lowest k value, so it has the lowest photocatalytic ability to methyl orange. Therefore, they are consistent with photocatalytic results (see Fig. 3).

3 Conclusions

$LaFe_{1-x}Mg_xO_3$ ($0 \leqslant x \leqslant 0.2$) ultrafine powders were synthesized by solution combustion method. Mg^{2+} doped in $LaFeO_3$ may forms solid solution, so it refine grain and increase specific surface area. Moreover, oxygen vacancies are formed in $LaFe_{1-x}Mg_xO_3$, wlich may promote separation of photoelectrons and holes. Therefore, these increase photocatalytic ability of the synthesized powders to methyl orange.

A suitable Mg^{2+} doping content in $LaFeO_3$ is the key to refining grain and decreasing particle agglomeration of the synthesized powders. Under the experimental conditions, when Mg^{2+} doping content is 0.1, $LaFe_{0.9}Mg_{0.1}O_3$ owns the highest specific surface area of 43.46 m^2/g and smaller particle size (100 nm and 150 nm in the diameter and length direction, respectively.). Therefore, it has the highest photocatalytic ability and degradation efficiency of methyl orange reaches 75.2% under the high-pressure mercury lamp irradiation for 180 min, and reaction may be described as the pseudo first order kinetics equation.

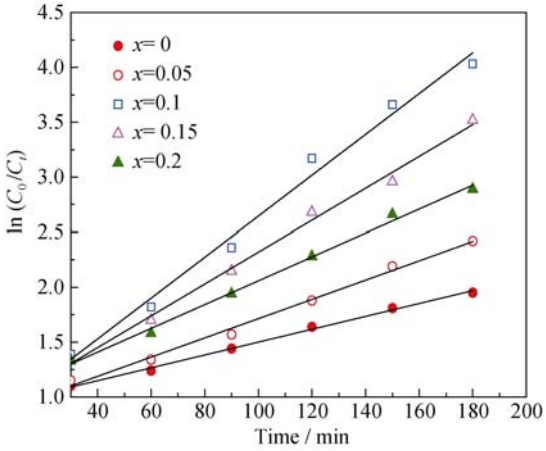

Fig. 4 Relationship between $\ln(C_0/C_t)$ and degradation time (t) of methyl orange with the synthesized $LaFe_{1-x}Mg_xO_3$ at different amount of Mg^{2+} doping

Table 2 Reaction equations and rate constant values for the degradation of methyl orange with the synthesized $LaFe_{1-x}Mg_xO_3$ at different Mg^{2+} doping contents

Doping content, x	Kinetic equation	Rate constant, k/min^{-1}	Correlation coefficient, R^2
0	$\ln(C_0/C_t)$=0.00587t+0.914	0.00587	0.9956
0.05	$\ln(C_0/C_t)$=0.00877t+0.83733	0.00877	0.9921
0.1	$\ln(C_0/C_t)$=0.0186t+0.78533	0.01860	0.9864
0.15	$\ln(C_0/C_t)$=0.01449t+0.87067	0.01449	0.9935
0.2	$\ln(C_0/C_t)$=0.01084t+0.97533	0.01084	0.9947

References:

[1] LI F T, LIU Y, LIU R H, *et al*. Preparation of Ca-doped $LaFeO_3$ nanopowders in a reverse microemulsion and their visible light photocatalytic activity. *Mater. Lett.*, 2010, **64(2):** 223–225.

[2] CUI Y R, LIU X Y, YUAN C L, *et al*. Preparation and properties of Sm_2O_3 doped $(Ba_{0.7}Ca_{0.3})TiO_3$-$Ba(Zr_{0.2}Ti_{0.8})O_3$ lead-free piezoelectric ceramics. *J. Inorg. Mater.*, 2012, **27(7):** 731–734.

[3] WANG B, CAO Q X, ZHANG S Y. Effects of the incorporation of Fe on the electromagnetic and microwave absorption performance of $La_{0.7}Sr_{0.3}MnO_3$ (+/- delta). *Mat. Sci. Semicon. Proc.*, 2014, **19:** 101–106.

[4] ABAZARI R, SANATI S. Perovskite $LaFeO_3$ nanoparticles synthesized by the reverse microemulsion nanoreactors in the presence of aerosol-OT: morphology, crystal structure, and their optical properties. *Superlattice Microst.*, 2013, **64:** 148–157.

[5] ZHANG Y M, LIN Y T, CHEN J L, *et al*. A high sensitivity gas sensor for formaldehyde based on silver doped lanthanum ferrite . *Sensor Actuat B-Chem.,* 2014, **190:** 171–176.

[6] SUN L P, RIEU M, VIRICELLE J P, *et al*. Fabrication and characterization of anode-supported single chamber solid oxide fuel cell based on $La_{0.6}Sr_{0.4}Co_{0.2}Fe_{0.8}O_3$-delta-$Ce_{0.9}Gd_{0.1}O_{1.95}$ composite cathode. *Int. J. Hydrogen Energy*, 2014, **39:** 1014–1022.

[7] MENG X, HAN D, WU H, *et al*. Characterization of $SrFe_{0.75}Mo_{0.25}O_3$-delta - $La_{0.9}Sr_{0.1}Ga_{0.8}Mg_{0.2}O_3$- delta composite cathodes prepared by infiltration. *J. Power Sources,* 2014, **246:** 906–911.

[8] HU R S, LI C, WANG X, *et al*. Photocatalytic activities of $LaFeO_3$ and La_2FeTiO_6 in p-chlorophenol degradation under visible light. *Catal. Commun.*, 2012, **29(5):** 35–39.

[9] PARIDA K M, REDDY K H, MARTHA S, *et al*. Fabrication of nanocrystalline $LaFeO_3$: an efficient Sol-Gel auto-combustion assisted visible light responsive photocatalyst for water decomposition. *Int. J. Hydrogen Energ.*, 2010, **35(22):** 12161–12168.

[10] KHODABAKHSH M, SEN C, KHASSAF H, *et al*. Strong smearing and disappearance of phase transitions into polar phases due to inhomogeneous lattice strains induced by A-site doping in $Bi_{1-x}A_xFeO_3$ (A: La, Sm, Gd). *J. Alloy Compd.*, 2014, **604:** 117–129.

[11] SUN X, DONG X T, WANG J X, *et al.* Fabrication and photocatalytic properties of $LaFeO_3$ nanobelts. *J. Chinese Ceram. Soc.,* 2012, **40(3):** 345–350.

[12] ZHENG J D, GE X T. Perovskite-type $SrFe_{1-x}Mn_xO_3$ catalysts: preparation by Co-precipitation method and catalytic performance for methane combustion. *Chinese. J. Inorg. Chem.,* 2013, **29(6):** 1307–1311.

[13] LI D, HUANG J F, CAO L Y, *et al*. Microwave hydrothermal synthesis of Sr^{2+} doped ZnO crystallites with enhanced photocatalytic properties. *Ceram. Int.*, 2014, **40(2):** 2647–2653.

[14] TORKIAN L, DAGHIGHI M. Effects of beta-alanine on morphology and optical properties of $CoAl_2O_4$ nanopowders as a blue pigment. *Adv. Powder Technol.*, 2014, **25(2):** 739–744.

[15] LIU F, HUANG J G, JIANG J H. Synthesis and characterization of red pigment $YAl_{1-y}Cr_yO_3$ prepared by the low temperature combustion method. *J. Eur. Ceram. Soc.*, 2013, **33(13/14):** 2723–2729.

[16] STRIKER T, RUUD J A. Effect of fuel choice on the aqueous combustion synthesis of lanthanum ferrite and lanthanum manganite. *J. Am. Ceram. Soc.*, 2010, **93(9):** 2622–2629.

[17] HU Z Q. Foundation Course of Inorganic Materials Science. Beijing: Chemical Industry Press, 2011**:** 56–71.

[18] GAO L, ZHENG S, ZHANG Q H. Photocatalytic Material of Nanometer Titania and Its Application. Beijing: Chemical industry Press, 2002**:** 238–258.

[19] LI G C, WANG Z M, SHI C, *et al*. Study on photocatalytic activity of $LaCoO_3$ ultrafine particle prepared by template method. *Chinese Rare Earths*, 2013, **34(4):** 35–40.

[20] RAO A N, SIVASANKAR B, SADASIVAM V. Kinetic study on the photocatalytic degradation of salicylic acid using ZnO catalyst. *J. Hazard. Mater*., 2009, **166(2/3):** 1357–1361.

溶液燃烧合成 $LaFe_{1-x}Mg_xO_3$ 超细粉体及其光催化性能

李家科, 刘 欣, 黄丽群, 王艳香

(景德镇陶瓷学院 材料科学与工程学院, 景德镇 333403)

摘 要: 采用溶液燃烧合成 Mg^{2+}掺杂 $LaFeO_3$ 超细粉体, 并利用 XRD、SEM、BET 和 UV-VIS 分析 Mg^{2+}掺杂量对合成粉体的物相组成、微观形貌和光催化性能的影响。结果表明: Mg^{2+}取代 Fe^{3+}形成 $LaFe_{1-x}Mg_xO_3$ ($0\leqslant x\leqslant 0.2$)有限型固溶体。当掺杂量为 0.1 时($x$=0.1), 合成粉体具有最大的比表面积(43.46 m^2/g)和较小粒径(径向和长度方向分别为 100 nm 和 150 nm), 因此具有最佳的光催化性能, 在高压汞灯 180 min 照射下, 对甲基橙溶液(10 mg/L)的降解率达 75.2%, 与纯 $LaFeO_3$ 的相比, 光降解率增加 26.5%, 且光催化反应符合一级动力学方程。

关　键　词: $LaFeO_3$; Mg^{2+}掺杂; 溶液燃烧法; 光催化性能

中图分类号: O614　　**文献标识码:** A